Simulated scanning tunneling microscopy images of few-layer phosphorus capped by graphene and hexagonal boron nitride monolayers

Pablo Rivero,[1] Cedric M. Horvath,[1] Zhen Zhu,[2] Jie Guan,[2] David Tománek,[2,*] and Salvador Barraza-Lopez[1,†]

[1]*Department of Physics, University of Arkansas, Fayetteville, Arkansas 72701, USA*

[2]*Physics and Astronomy Department, Michigan State University, East Lansing, Michigan 48824, USA*

(Received 18 December 2014; revised manuscript received 16 February 2015; published 10 March 2015)

Elemental phosphorous is believed to have several stable allotropes that are energetically nearly degenerate, but chemically reactive. These structures may be capped by monolayers of hexagonal boron nitride (h-BN) or graphene to prevent chemical degradation under ambient conditions. We perform *ab initio* density functional calculations to simulate scanning tunneling microscopy (STM) images of different layered allotropes of phosphorus and study the effect of the capping layers on these images. At scanning energies within its intrinsic conduction gap, protective monolayers of insulating h-BN allow to distinguish between the different structural phases of phosphorus underneath due to the electronic hybridization with orbitals from the upmost phosphorus atoms: h-BN capping monolayers thus provide a promising route to tell few-layer phosphorus allotropes from one another with local probes.

DOI: 10.1103/PhysRevB.91.115413 PACS number(s): 68.37.Ef, 31.15.A−, 73.90.+f

I. INTRODUCTION

There has been an unprecedented interest in layered phosphorus allotropes as a new member of the family of two-dimensional (2D) materials in the post-graphene era [1,2]. The interest has been triggered by reports indicating that layered bulk black phosphorus [3–11] can be exfoliated mechanically yielding few-layer phosphorene, a novel 2D material with a significant fundamental band gap and a high carrier mobility [12–15] exceeding that of transition metal dichalcogenides ($MX_2's$) [16]. Few-layer phosphorene bears promise for intriguing optoelectronics applications [17] since the fundamental band gap can be tuned by the number of layers and by in-layer stretching or compression [12,18–23]. But what truly sets phosphorene apart from other 2D systems is its polymorphism: Besides the well-studied black phosphorus allotrope, energetically near-degenerate alternate structures have been postulated including blue phosphorus, γ-P, δ-P, and their combination in one layer [24–32]. Identifying and discriminating between these structures requires a tool capable of probing structures in real space with subnanometer resolution. Scanning tunneling microscopy (STM) is such an ideal tool, but scanning requires having chemically stable samples.

Even though phosphorene is known to degrade under ambient conditions [14,33,34], significant progress has been achieved in its stabilization by passivating the exposed surface [35]. In the initial transport studies this passivation has been achieved by a thick PMMA coating [12–15] that, of course, precludes an STM study of the underlying structure. Besides PMMA, however, monolayers of graphene and hexagonal boron nitride (h-BN) [36–38] have proven effective in this sense, constituting the thinnest "galvanizing agents." Capping by h-BN or graphene monolayers has also been shown to protect phosphorene from degradation [34,39]. Similar to graphene, h-BN is a chemically inert material that can be exfoliated from bulk materials by mechanical transfer [40–43] or can be synthesized by chemical vapor deposition [44]. Unlike in semimetallic graphene, the observed fundamental band gap of h-BN is very large and close to 6 eV [45].

Even though a structure may be capped by a passivating graphene monolayer, it has been established that the underlying structure can be revealed by STM imaging [46], and the main objective of this computational study is to establish whether different phosphorene allotropes can also be distinguished in STM studies when covered by a monolayer of h-BN or graphene. If so, then STM may also be able to reveal line defects including disclinations [47] and grain boundaries separating different phases in the underlying phosphorene layer [48]. The nature and concentration of defects is critical for the stability of phosphorene since defects act as nucleation sites in the material degradation process.

Calculations have been carried out using the SIESTA *ab initio* simulation package [49] with a cutoff energy of 300 Ry. The optB88-vdW local exchange functional [50] was used to describe van der Waals interactions among successive layers. Norm-conserving Troullier-Martins pseudopotentials [51] and a double-ζ basis including polarization orbitals were employed in calculations. Structural relaxations were performed using the conjugate gradient method until the atomic forces were below 0.04 eV/Å. The electron densities were integrated over dense k-point meshes using an in-house program, and visualized with the *Denchar* program.

II. RESULTS AND DISCUSSION

A. Equilibrium geometry and structural stability of capped phosphorus slabs

We first determined the equilibrium geometry of thin slabs of multilayer phosphorene capped on both sides with passivating hexagonal boron nitride or graphene monolayers as shown in Fig. 1. We considered five-layer slabs of black phosphorus (black P), blue phosphorus (blue P), δ phosphorus (δ-P), and γ phosphorus (γ-P) [24,25,52–54] with no relative in-plane displacements nor rotational faults. The fundamental band gap, and the optimum interlayer separation l defined in

*tomanek@pa.msu.edu

†sbarraza@uark.edu

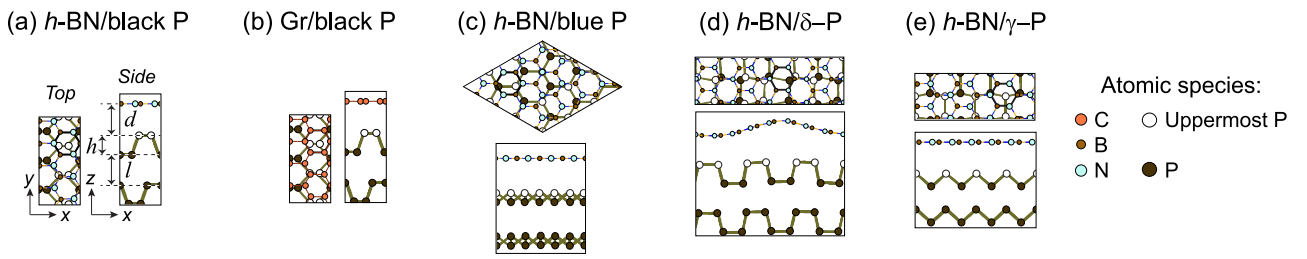

FIG. 1. (Color online) Atomistic structure of five-layer phosphorene slabs capped with hexagonal boron nitride (h-BN) or graphene (Gr) monolayers (only the two uppermost phosphorene layers and one capping monolayers are shown). As it will turn out, we will be unable to register significant phosphorene features through graphene at an equilibrium relative separation in our STM simulations. In addition, the structures capped by h-BN or graphene are quite similar [c.f. structures (a) and (b)]; only their relative separation d changes (c.f. Table II). For these two reasons, only one structure capped by graphene is shown on this figure [structure (b)].

Fig. 1, approach their limiting bulk values at this thickness already [25]. The idea here is to create systems small enough that, at the same time, could be representative of bulk samples. This choice will thus aid experimental searches of different phases on thick slabs.

Keeping the optimum unit cell size of the 2D phosphorene slab, we capped the slabs by a h-BN or a graphene monolayer on both sides to suppress spurious dipole effects. The equilibrium geometry of most structures considered is reproduced in Fig. 1, with only two layers of the five-layer phosphorene slabs shown in the structural side views. The coloring of atomic species is as follows: the atoms in the top P layer that are closest to the capping monolayers are shown in white (closest P); all other P atoms are shown in brown. N atoms can be seen in light blue, B atoms in orange, and C atoms in red. Black phosphorene, δ-P, and γ-P have rectangular unit cells and Brillouin zones [25], whereas blue phosphorene has a hexagonal unit cell and Brillouin zone reminiscent of graphene [24].

The size of the supercells, listed in Table I, ranges from 92 to 184 atoms. The average distance d between the topmost P atoms (shown in white in Fig. 1) and the h-BN or graphene capping layer is listed in Table II and it ranges from 3.55 Å in γ-P to 3.89 Å in δ-P. Since the equilibrium lattice constant of h-BN and graphene monolayers differs in between 0.1 and 7.0% from that of the phosphorus slabs (Table I), the capping layers have been stretched or compressed to enforce epitaxy. In the δ-P slab, the h-BN overlayer shows an energetic preference for a wavy structure [55]—shown in Fig. 1(d)—over a planar compressed structure, displaying a pattern reminiscent of the observed structure in slabs of phosphorus IV [56].

It is important to note that not all phosphorene slabs were capped with graphene in the present study. This is so mainly because graphene's large nonzero electron density at relevant scanning energies precludes the use of these slabs for semiconductor applications, and because graphene's nonzero electronic density may obscure a simple identification of phosphorene phases underneath.

We investigated the adhesion of the capping layer on the phosphorus slab. We defined the adhesion energy $E_{\rm ad}$ by

$$E_{\rm ad} = (1/2)[E_{\rm tot}(\text{capped P slab}) - 2E_{\rm tot}(\text{capping layer}) - E_{\rm tot}(\text{P slab})]. \quad (1)$$

Here, $E_{\rm tot}$(capped P slab) is the total energy of the P slab capped by either h-BN or graphene at both exposed surfaces, $E_{\rm tot}$(P slab) is the total energy of the isolated P slab, and $E_{\rm tot}$(capping layer) is the energy of a single monolayer of h-BN or graphene. Negative values indicate energy gain upon adhesion, and the factor 1/2 takes care of the fact that the slab is capped at both sides. We find it useful to divide the adsorption energy by the interface area A and list the values of $E_{\rm ad}/A$ in Table II. h-BN/black P turns out to be the most stable capped system, with an energy gain upon adhesion of 21.60 meV/Å^2. h-BN/δ-P has the weakest adhesion energy (19.49 meV/Å^2) among h-BN capped systems, which is caused by a larger average separation between h-BN and the wavy phosphorene layer, as seen in Fig. 1(d). When phosphorene slabs are capped by graphene monolayers the adhesion energy becomes weaker than on their h-BN-capped counterparts, as evidenced by a comparison of values of $E_{\rm ad}/A$ among pairs of columns (e.g., h-BN/black P and

TABLE I. Cell parameters and number of atoms per unit cell in phosphorus allotropes capped by h-BN or graphene (Gr) monolayers. The lattice constants are $a_g = 2.49$ Å for Gr and $a_{\rm BN} = 2.52$ Å for h-BN. No STM imaging of structures δ-P and γ-P capped by graphene was pursued on this work.

System:	black P		blue P	δ-P		γ-P	
Cell parameters (Å):	4.58,	10.05	9.97	16.51,	5.43	13.60,	5.35
h-BN mismatch (%):	1.1,	0.3	4.7	7.0,	−5.5	3.8,	5.9
Gr mismatch (%):	5.7	0.9	0.1	–	–	–	–
Supercell size:	1 × 3		3 × 3	3 × 1		4 × 1	
Number of atoms:	92		154	184		128	
Number of P atoms:	60		90	120		80	

TABLE II. Structural information and adhesion energy E_{ad} of five-layer phosphorene slabs capped by h-BN or graphene (Gr). As defined in Fig. 1, the average closest distance among P atoms (in white in the structural models) and the h-BN or graphene monolayer is d, the average thickness of the P layer is h, and the average interlayer separation on the P slabs is l. E_{ad}/A is the adsorption energy E_{ad} of the capping layer on the phosphorus substrate defined in Eq. (1), divided by the area of the unit cell A. Neither δ nor γ structures capped with graphene were pursued on this study.

	h-BN/black P	Gr/black P	h-BN/blue P	Gr/blue P	h-BN/δ-P	h-BN/γ-P
d (Å)	3.68	3.56	3.75	3.60	3.89	3.55
h (Å)	2.19	2.19	1.27	1.27	2.24	1.61
l (Å)	3.58	3.42	3.68	3.58	3.33	2.40
E_{ad}/A (meV/Å^2)	−21.60	−20.38	−20.26	−18.02	−19.49	−20.62

Gr/black P, or h-BN/blue P and Gr/blue P in Table II). We discuss the electronic properties of these slabs next.

B. Electronic properties of capped phosphorus slabs

The Fermi level of capped phosphorene slabs is set at $E_F = 0$ eV. We provide band structures, the total density of states, and the electronic density projected onto atoms belonging to the capping monolayers in Fig. 2. Graphene has a zero band gap and the DFT value of the fundamental band gap of an isolated h-BN monolayer is 4.5 eV. We determine a band gap of 0.44 eV for black P, 0.84 eV for blue P, and 0.21 eV for δ-P slabs, with the γ-P slab being metallic [25] (c.f., Fig. 2). These gaps are further emphasized in the total density of states (DOS) plots shown to the right of each band structure plot. In slabs made with two semiconductors [Figs. 2(a), 2(c), and 2(e)], we set the Fermi energy at the midgap among phosphorene states.

The relative alignment of the nominal band-gap edges of h-BN is shown by thick (red) horizontal lines, and the relative energy of these band edges is clearly sensitive to the relative separation Δz among h-BN and the phosphorene slab underneath, as indicated by the feeble dash horizontal line in Fig. 2(a) obtained when h-BN pushed by 0.4 Å down into black P. Additionally, an evident orbital hybridization as a function of Δz into electronic states within the nominal band gap has been highlighted by the tilted arrows in Fig. 2(a). We will discuss hybridization in full detail later on.

The gray (dashed) rectangles in all plots indicate the energy window in which STM imaging will take place; the red horizontal lines on h-BN capped phosphorene allotropes indicate that the STM scanning window is located within the nominal gap of an isolated h-BN monolayer [Figs. 2(a), 2(c), 2(e), and 2(f)]. As it is known, graphene has a nonzero electronic density in all scanning windows [Figs. 2(b) and 2(d)].

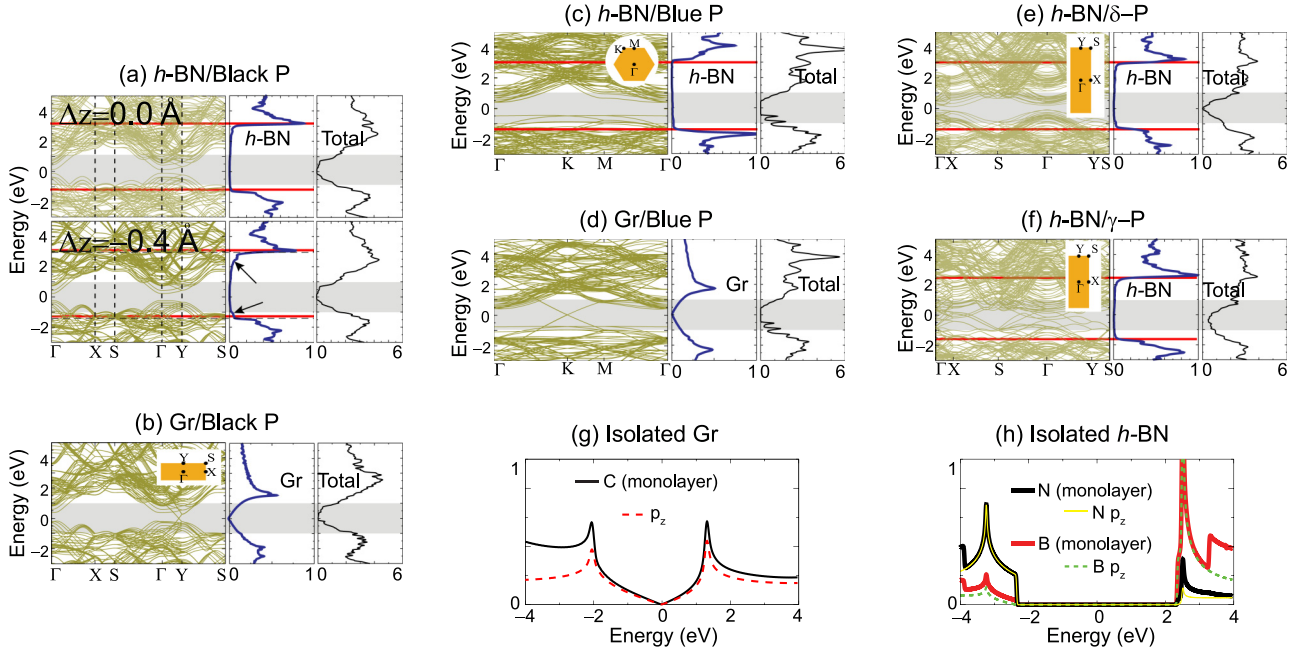

FIG. 2. (Color online) Electronic structure properties of five-layer phosphorene slabs capped with hexagonal boron nitride (h-BN, subplots a,c,e, and f) and graphene (subplots b and d) monolayers. Electronic bands are in the left subpanels, and Brillouin zones are seen as insets of these plots. The arrows in subplot a for $\Delta z = -0.4$ Å indicate a clear hybridization within the nominal gap of h-BN. This hybridization produces a height-dependent shift of the band edges that is clearly seen in subplot (a) by comparing the bold red and the thin horizontal dashed lines. Although less visible, such hybridization occurs for all h-BN capped slabs. The projected h-BN and total density of states are shown in the right subpanels. The density of states for isolated graphene and for h-BN, and their projections into p_z orbitals are displayed in the (g) and (h) subplots.

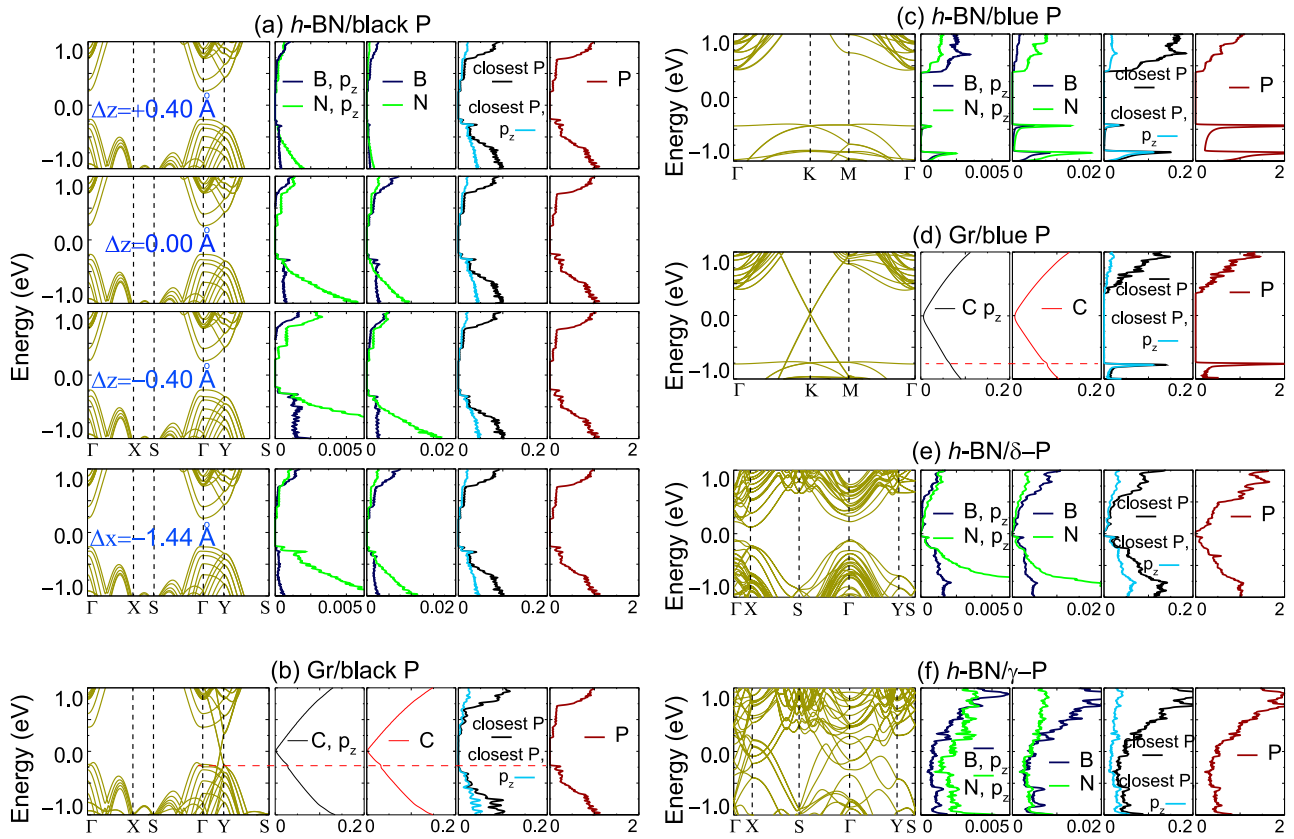

FIG. 3. (Color online) Band structures and projected density of states onto B, N, C, and P atoms within ±1 eV for phosphorene slabs capped by *h*-BN and graphene monolayers. Note that *h*-BN hybridizes with phosphorus states within its nominal band gap (c.f. Table III). Graphene states in capped structures exhibit an intrinsic charge that is one order of magnitude larger than the charge induced on *h*-BN by hybridization, and only shallow additional hybridization by phosphorene is visible in subplots (b) and (d), as highlighted by horizontal dashed lines. The hybridized states shown here are those observed on STM images in Figs. 4 to 7.

We indicate the total density of states and its projection onto the p_z channel for isolated *h*-BN [57] and graphene in Figs. 2(g) and 2(h) as well, as the distribution of p_z orbitals among B, N, and C atoms may shed light on the complex hybridization taking place when these monolayers are in close proximity to phosphorene allotropes at this energy window. While graphene is known to have a π (p_z) orbital character around the Fermi energy [c.f. Fig. 2(g)], the valence (conduction) band of *h*-BN has a predominant N (B) p_z character [c.f. Fig. 2(h)]. There is a subtle hybridization of the *h*-BN monolayer on these phosphorene slabs that is discussed next.

The energy range in Fig. 2 was made sufficiently large in order to capture the nominal band edges of *h*-BN, but we have obtained STM images within ± 1 eV from the Fermi energy (dashed rectangles in Fig. 2), making it important to look at the electronic states at this energy window to better understand the electronic states seen on STM images. In Fig. 3, we correlate band structure features with atomic species and orbital character through projected density of states plots for energies relevant to our STM images, that will be discussed later on.

For this purpose, the total density of P atoms is shown on the rightmost subplots in Fig. 3, and the electronic density projected onto the P atoms closest to the capping monolayers (seen in white in Fig. 1) has been recorded too. We registered the p_z character of these orbitals too, finding a relatively larger p_z character for the P orbitals with negative energies [c.f. Figs. 3(a) to 3(f)].

While—by definition—an isolated *h*-BN monolayer has a zero electron density for energies within its electronic gap [Fig. 2(h)], this ceases to be the case as soon as the slab is in proximity of other material with a smaller gap: *h*-BN has a nonzero electronic density due to hybridization with the closest P atoms [Figs. 2(a), 2(c), 2(e), and 2(f); this is more clearly seen in Figs. 3(a), 3(c), 3(e), and 3(f)]. Furthermore, it is crucial to emphasize the density scale of the hybridized *h*-BN monolayers, which is an order of magnitude smaller than that set for the closest P atoms and graphene (the density scale of electron per unit cell is consistent among Figs. 2 and 3). The density scale for graphene is identical to that of the closest P atoms, and this could preclude an easy identification of P-related features for graphene-capped phosphorene. One notes that the hybridization seen on *h*-BN follows the same pattern seen in Fig. 2(h). Namely, states with negative energies have a predominant N character, while states with positive energies display a larger B character. The only exception to this trend is realized in blue phosphorene, Fig. 3(c), which indicates the role of structure and symmetries on the resulting hybridization. An additional piece of information concerns the orbital projection onto p_z orbitals on *h*-BN, which is almost an order of magnitude smaller than the overall density recorded

TABLE III. Total charge ΔQ in electrons per unit cell, and percentage charge distribution into s and p orbitals within a -1 to 1 V bias window for phosphorene slabs capped by hexagonal boron nitride (h-BN) or graphene (Gr) monolayers. The hybridization on h-BN under forward bias is mostly localized on N p_z channels. Graphene-capped materials have a large intrinsic charge on the C p_z orbitals that will mask the electronic density of the P slabs underneath on STM images.

System:	h-BN/black P, $\Delta z = +0.4$ Å				h-BN/black P, $\Delta z = 0.0$ Å				h-BN/black P, $\Delta z = -0.4$ Å			
Bias window (V):	$(-1,0)$		$(0,+1)$		$(-1,0)$		$(0,+1)$		$(-1,0)$		$(0,+1)$	
ΔQ (e/uc):	0.001		0.001		0.004		0.002		0.006		0.003	
Atomic species:	B	N	B	N	B	N	B	N	B	N	B	N
s (%):	16	3	16	1	10	6	3	2	9	6	1	2
p_x and p_y (%):	20	0	0	0	15	0	0	1	12	1	0	3
p_z (%):	14	17	20	52	12	31	15	60	13	35	15	62
System:	h-BN/black P, $\Delta x = +1.44$ Å				Gr/black P				h-BN/blue P			
Bias window (V):	$(-1,0)$		$(0,+1)$		$(-1,0)$		$(0,+1)$		$(-1,0)$		$(0,+1)$	
ΔQ (e/uc):	0.003		0.003		0.092		0.105		0.001		0.003	
Atomic species:	B	N	B	N	C		C		B	N	B	N
s (%):	12	5	6	2	0		0		7	0	9	3
p_x and p_y (%):	17	1	1	1	0		0		26	0	20	0
p_z (%):	19	17	6	78	89		86		30	15	18	20
System:	Gr/blue P				h-BN/Delta P				h-BN/Gamma P			
Bias window (V):	$(-1,0)$		$(0,+1)$		$(-1,0)$		$(0,+1)$		$(-1,0)$		$(0,+1)$	
ΔQ (e/uc):	0.076		0.083		0.013		0.003		0.009		0.021	
Atomic species:	C		C		B	N	B	N	B	N	B	N
s (%):	0		0		11	5	0	0	4	0	3	0
p_x and p_y (%):	0		0		14	3	1	3	9	0	7	0
p_z (%):	86		86		13	23	10	69	12	14	10	22

on h-BN at these energies, and implying contributions from other orbitals to these hybridized states as well (c.f. Table III).

Electronic hybridization implies charge transfer. A slight electron/hole charge transfer sets the Fermi energy right at the conduction/valence-band edge in an isolated system. However, h-BN is not isolated in Fig. 1; it is in close proximity to phosphorene slabs that induce a small electronic hybridization within its otherwise empty nominal electronic gap. This slight hybridization of electronic states within the nominal gap of h-BN is documented on subplots B and N in Figs. 3(a), 3(c), 3(e), and 3(f), as well as in Table III: phosphorene slabs transfer a small electronic charge ΔQ to the h-BN monolayer, and this orbital hybridization allows for a gradual band shift of h-BN with respect to the phosphorene slab as a function of d. This effect will be explored further in the next paragraph, when h-BN is intentionally pulled towards/away from the black phosphorene slab, but a similar slight hybridization was reported in weakly adsorbed carbon nanotubes on Si some time ago [58].

When an STM samples a layered material, it pushes/pulls it away from its equilibrium atomistic configuration as it attempts to establish a feedback current [46], so the alignment of the h-BN electron bands with respect to those of the phosphorene slabs further depends on the relative distance d between h-BN and the phosphorene slab. This effect is studied here in detail: We register small band shifts of the h-BN with magnitudes -0.265, -0.166, -0.075, $+0.045$, and $+0.075$ eV with respect to the band alignment shown in Fig. 2(a), upper subplot ($\Delta z = 0.0$ Å), as the h-BN monolayer is vertically displaced by a distance $\Delta z = -3.0$, -0.4, -0.2, $+0.2$, or $+0.4$ Å away from the black P slab, with respect to its equilibrium atomistic separation d in Fig. 1(a) that has a value of $\Delta z = 0$ Å. The dashed horizontal lines seen with the naked eye on Fig. 2(a), subplot $\Delta z = -0.4$ Å confirm this observation. Structural defects or chemical contamination will cause additional relative band shifts.

Additional details on the mechanism responsible for the slight band shift seen in Fig. 2(a) can be found by contrasting subplots $\Delta z = +0.4$, 0.0, and -0.4 Å in Fig. 3(a): it is clear from these figures that the hybridization on B and N is largest—implying the larger charge transfer that is reported on Table III—the closest they are to the phosphorene slab ($\Delta z = -0.4$ AA); this is emphasized by using the same scale in the PDOS for h-BN for all subplots in Fig. 3.

In Table III, we integrate the electronic charge ΔQ onto B, N, or C electronic orbitals within 1-V bias windows from E_F. ΔQ is certainly nonzero, ranging in between 0.001 and 0.021 electrons per unit cell for h-BN capped slabs, and between 0.076 and 0.105 electrons per unit cell for graphene-capped slabs. The slight difference in charge for graphene arises mainly from the well-known Fermi velocity renormalization, due to the different magnitudes of strain employed to enforce epitaxy in black P and in blue P (c.f. Table I). The important points are that (i) the total charge within the nominal gap for h-BN is nonzero due to orbital hybridization and (ii) graphene has an intrinsic charge that is an order of magnitude higher, which will preclude a clear-cut observation of P-related features within the STM scanning energy window [phosphorene features may be visible at the energies shown by horizontal dashed lines in Figs. 3(b) and 3(d); still, it will be simpler to tell phsophorene allotropes through h-BN, as it will be shown later on].

The phosphorus atom wave functions hybridize the orbitals of the capping layer. For h-BN, it is precisely these hybridized

orbitals that become observable in STM images to be shown later on. Graphene has an electronic density that is comparable with that of the closest phosphorene atoms: since the STM image is captured over graphene and farther away from the phosphorene slabs, graphene contributes a larger electron density in these systems; this is at variance with what is observed in III-V semiconductors, where surface states still overcome the density of graphene at the relevant scanning energies [46]. (The effect is material-dependent, as it may be expected.)

Additional information in Table III indicates how the charge projects among the s and p orbitals of the capping slabs. Without exception, all slabs capped with h-BN have a larger density on their N p_z orbitals while under forward bias (negative energies) as it was seen in Figs. 2(h) and 3. In the case of reverse bias, this preponderance is not as marked: one even observes a slightly larger density onto the B p_z orbital when h-BN is horizontally displaced by $\Delta x = 1.44$ Å on black P, as the registry among P and B atoms is enhanced there.

On graphene-capped monolayers, the s and the in-plane p orbitals contribute no electron density, while almost 90% of the density is projected onto p_z orbitals that form the carbon π bond, and we register a slight ∼10% contribution from the d orbitals in the atomic-based basis set to such density (c.f. Table III). Although the p_z contribution in hybridized h-BN is still dominant, nonzero contributions from the s, p_x, and p_y orbitals can be registered at these biases. Additionally, the contribution of d orbitals to the total charge can be computed by substracting 100% to the sum of values in Table III. For instance, the contribution of d orbitals is 19% (26%) under forward (reverse) bias for the h-BN/Black P system with $\Delta z = 0.0$ Å. While protecting phosphorene from chemical degradation, h-BN will permit the identification of atomistic features of the phosphorene structure, as will be discussed later.

C. Simulation of STM images

It is well established that STM images can be simulated by *ab initio* density functional calculations [59]. Applying a small bias voltage V_{bias} between the sample and the STM tip yields a tunneling current, whose density $j(\mathbf{r})$ can be obtained from a simple extension [60] of the expression derived by Tersoff and Hamann [61,62]:

$$j(\mathbf{r}, V_{\text{bias}}) \propto \rho_{\text{STM}}(\mathbf{r}, V_{\text{bias}}) \,, \tag{2}$$

where

$$\rho_{\text{STM}}(\mathbf{r}, V_{\text{bias}}) = \int_{E_F - eV_{\text{bias}}}^{E_F} dE \rho(\mathbf{r}, E) \tag{3}$$

and

$$\rho(\mathbf{r}, E) = \sum_{n,\mathbf{k}} |\psi_{n\mathbf{k}}(\mathbf{r})|^2 \delta(E_{n,\mathbf{k}} - E) \,. \tag{4}$$

Here, $\rho(\mathbf{r}, E)$ is the local density of states at the center of curvature of the tip at $\mathbf{r}$ and $\psi_{n\mathbf{k}}(\mathbf{r})$ are the electron eigenstates of the unperturbed surface at energy $E_{n,\mathbf{k}}$. These eigenstates are commonly represented by Kohn-Sham eigenstates obtained using density functional theory. The implied assumptions [60–62] are that the relevant tip states are well described by

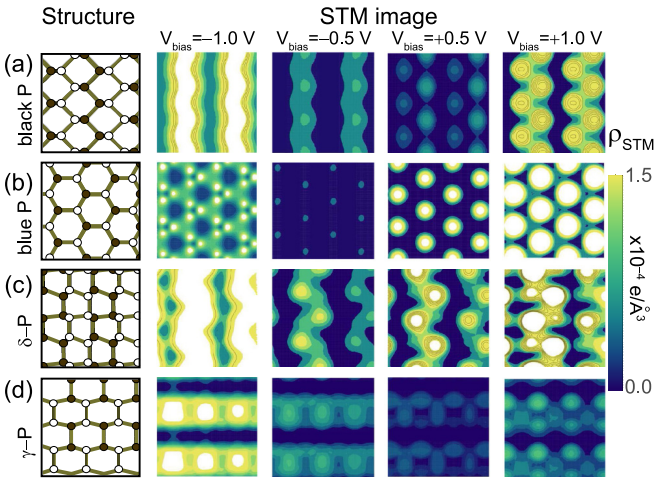

FIG. 4. (Color online) Simulated STM images of a 10×10 Å area of bare (a) black phosphorene, (b) blue phosphorene, (c) δ-P, and (d) γ-P slabs. Presented is ρ_{STM} at constant height, corresponding to the current imaging mode, at different values of the bias voltage V_{bias}. For the sake of simple comparison, the geometry of the topmost two layers of the slabs is reproduced to scale in the left panels, with topmost atoms shown in white. Streaks seen on black phosphorene, δ-P and γ-P reflect their "ridged" atomistic structure, also highlighted in the structural models. The different threefold symmetry of blue phosphorene with a triangular sublattice, associated with the white-colored P atoms in the topmost layer, is clearly reflected in the STM images in (b).

s waves with a constant density of states. Furthermore, the tunneling matrix element is considered to be independent of the lateral tip position for a constant tip-to-surface distance and also independent of the bias voltage V_{bias} in the narrow (but nonzero) energy region $[E_F - eV_{\text{bias}}, E_F]$. Whereas Eq. (3) describes tunneling from occupied states of the sample to the tip, an obvious change of this expression can describe tunneling from the tip to unoccupied states in the energy range $[E_F, E_F + e|V_{\text{bias}}|]$. This latter configuration is referred to as reverse bias and described by a negative bias voltage.

D. Simulated STM images of bare few-layer phosphorene slabs

Simulated STM images of bare few-layer phosphorene slabs, representing the charge density $\rho_{\text{STM}}(\mathbf{r}, V_{\text{bias}})$, given by Eq. (3), at various bias voltages V_{bias} are presented in Fig. 4. For better interpretation of the images, we reproduced the atomic arrangement in the topmost layers of the slab in the left panels. Visual comparison of the structures and the STM images reveals that the highest values of ρ_{STM} correlate well with the location of the topmost P atoms, which are shown in white in the structural depiction. Underlying all STM images is a dense k-point mesh used in Eq. (4) for the charge density integration. The STM image is represented by ρ_{STM} scanned within a plane at the distance $d = 2.3$ Å from the closest phosphorus atoms shown in white. For the sake of simple comparison, we keep the scan area and the color bars the same in Figs. 4 to 7.

An antibondinglike feature is visible by the spatial distribution localized over P atoms at forward bias V_{bias} on black

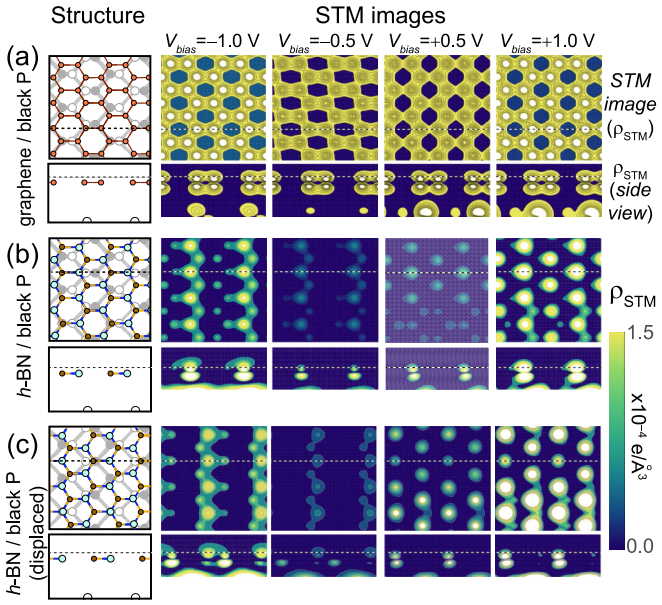

FIG. 5. (Color online) Simulated STM images of a 10×10 Å area of a black phosphorene slab capped by a monolayer of (a) graphene, (b) h-BN and (c) a horizontally displaced h-BN monolayer. Presented is ρ_{STM} at constant height, corresponding to the current imaging mode, at different values of the bias voltage V_{bias}. The lower subpanels represent ρ_{STM} in a plane normal to the surface. For the sake of simple comparison, the geometry of the topmost layers of the slabs is reproduced to scale in the left panels, with topmost P atoms shown in white. The ridged structure of black P, which is clearly visible in Fig. 2(a) at $V_{bias} = -1.0$ V, is completely obscured by a graphene layer in (a), but is visible underneath an h-BN layer in (b) and (c).

P [Fig. 4(a)]. On the other hand, a bondinglike feature is reproduced under a negative bias as the electronic density is larger at bonds between pairs of P atoms. In blue phosphorus [Fig. 4(b)], a triangular shape of the electronic density is seen under forward bias due to the electronic density coming only from the upper P atoms. The images under a reverse bias $V_{bias} = -1V$ show a decorated triangular lattice displaying three bright small circles around each uppermost (white) P atom. The higher intensity for $V_{bias} > 0$ correlates with the rather flat valence band seen on Fig. 3(c) (the reader must divide the energy scale in Figs. 2 and 3 by $-|e|$ to obtain V_{bias} on Figs. 4 to 7).

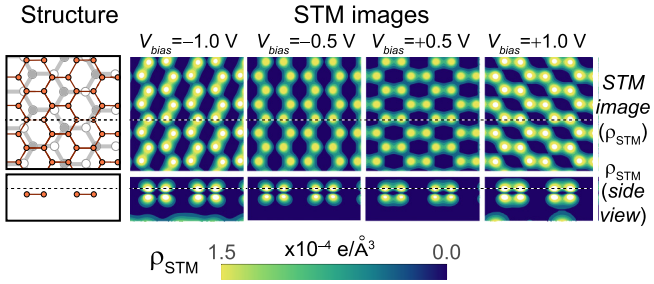

FIG. 6. (Color online) Simulated STM images of a 10×10 Å area of a blue phosphorene slab capped by a graphene monolayer.

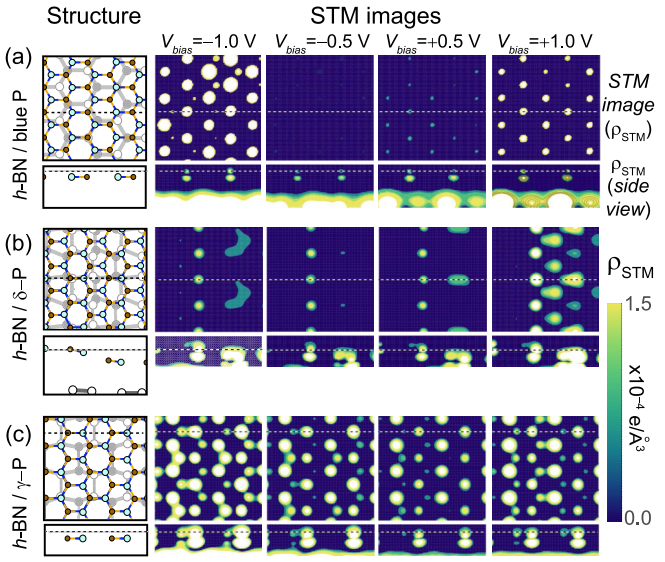

FIG. 7. (Color online) Simulated STM images of a 10×10 Å area of a (a) blue phosphorene, (b) δ-P, and (c) γ-P slab capped with an h-BN monolayer. Presented is ρ_{STM} at constant height, corresponding to the current imaging mode, at different values of the bias voltage V_{bias}. The lower subpanels represent ρ_{STM} in a plane normal to the surface. For the sake of simple comparison, the geometry of the topmost layers of the slabs is reproduced to scale in the left panels, with topmost P atoms shown in white.

Two vertical trenches can be seen in δ-P [Fig. 4(c)] for forward and reverse biases, but the shape of these trenches is different depending on bias direction: The electronic density ρ_{STM} is localized onto the upper P atoms for positive V_{bias}, and it appears more distributed over bonds under reverse biases; this is particularly evident for $V_{bias} = -1V$. The spatial density acquired above the γ-P slab also exhibits two horizontal trenches under negative bias in a bondinglike fashion as the charge is distributed away from atoms and into covalent bonds [Fig. 4(d)]. Due to the antibondinglike distribution, these electronic density trenches can be seen localized over the P atoms when $V_{bias} > 0$ V.

Clearly, different structural phases can be distinguished with an STM. Next, we will study if these structures remain distinguishable by STM when covered by a capping monolayer.

E. Simulated STM images of few-layer phosphorus slabs capped by *h*-BN or graphene

Simulated STM images of few-layer black phosphorene slabs capped by h-BN or graphene are presented in Fig. 5. In the current imaging mode, the STM current is represented by the charge density $\rho_{STM}(\mathbf{r}, V_{bias})$, given by Eq. (3). We present ρ_{STM} at various bias voltages V_{bias} in a plane parallel to the surface, indicated by a dashed horizontal line in the structural image in side view. We also present ρ_{STM} in a plane normal to the surface, indicated by a dashed horizontal line in the structural image in top view. These images allow us to judge, whether the structure of a phosphorene slab may be distinguished underneath a capping monolayer of h-BN or graphene.

The STM images in Figs. 5(b) and 5(c) indicate that the *h*-BN layer allows, to some degree, to discriminate between different phosphorene phases [26]. As a result of the small but finite hybridization, the white/yellow streaks in STM images in Fig. 4(a) seen at $V_{\text{bias}} = -1.0$ V—highlighting the ridges of a black phosphorene surface—become visible underneath the *h*-BN layer in Figs. 5(b) and 5(c).

In the case of III-V semiconductors, a capping monolayer of graphene, when pushed by the STM tip to close proximity of the substrate, was found to not to conceal the atomic structure of the substrate [46]. That experimental observation made us consider whether phosphorene could be seen through graphene/*h*-BN. As seen in Fig. 4(a), this is clearly not the case for black phosphorene covered by graphene. Independent of the bias voltage, the simulated STM images are dominated by the structure of the graphene overlayer. The significantly larger density of graphene states in the scanning plane efficiently masks the ridged structure of black phosphorene, which is most clearly visible in the STM image of the bare surface at $V_{\text{bias}} = -1.0$ V on Fig. 5(a). Also, the side view images—cut along a carbon covalent bond—show a symmetric distribution of the electronic density of the π bond among pairs of carbon atoms. In addition, one sees in Fig. 6 an overwhelming contribution from graphene states as well. We could push graphene to the slab and hope to see a similar effect to that reported in Ref. [46], but there may be a simpler way to protect phosphorene and determining the layered phase at the exposed surface: In contrast to the semimetallic graphene, *h*-BN will indeed permit the identification of the phosphorene allotrope underneath. Based on these results, we did not consider graphene-capped δ-P and γ-P here.

To further understand the differences between Figs. 4(a) and 5(b), caused by the presence of the capping *h*-BN layer, we invite the reader to observe the contributions from hybridized B and N atoms onto the STM images, as given by Fig. 3 and Table III.

Even though the adhesion of the *h*-BN layer on the phosphorene substrate is substantial according to Table II, contact with the STM tip may shift the capping layer horizontally. In the following, we discuss the effect of such a horizontal displacement on the STM image. Figures 5(b) and 5(c) both represent a black P slab covered by *h*-BN; the capping layer in 5(c) has been shifted from its position in 5(b). This displacement can be visualized most easily in the side view of the atomic structure, in a plane normal to the surface. As seen at the top of the left panels in Figs. 5(b) and 5(c), this plane contains two P atoms in the topmost P layer. At the bottom of the left panels of these subfigures, we can see the effect of a horizontal displacement by 1.44 Å. One of the P atoms, which was underneath an N atom in Fig. 5(b), appears underneath a B atom in 5 c. Even though this displacement represents the worst-case scenario of switching from P-N registry to P-B registry, the STM images in Figs. 5(b) and 5(c) are rather similar at all bias voltages, indicating image stability with respect to displacements of the capping layer. In particular, the ridged structure, which dominated the image of the bare surface in Fig. 4(a), still appears pronounced on Figs. 5(b) and 5(c).

It is time to establish from the STM images, whether graphene allows the identification of phosphorene allotropes underneath. One can only see graphenelike features in Figs. 5(a) and 6. This means that, even if graphene hybridizes with phosphorene states [dashed horizontal lines on Figs. 3(b) and 3(d)], telling blue P from black P does not seem straightforward when these slabs are capped by a graphene monolayer. On the other hand, *h*-BN will permit identification of phosphorene allotropes, as it will be shown next.

We simulated STM images of blue P, δ-P, and γ-P to judge whether the different allotropes can be distinguished underneath an *h*-BN monolayer. We find these images, presented in Fig. 7, to be all different, and to also differ from those of black P in Figs. 5(b) and 5(c). In comparison to black P with a rectangular unit cell, Fig. 7(a) clearly reveals the honeycomb lattice of the underlying blue phosphorene. Similarly, ρ_{STM} of a capped δ-P slab in Fig. 7(b) displays two vertical stripes at locations above N atoms at negative bias values, in close agreement with Fig. 4(c). Due to its wavy morphology, the capping layer binds least to the substrate and is most likely to be displaced by an STM tip during scanning. The STM images of a capped γ-P slab, shown in Fig. 7(c), display similar ridges as seen in the bare γ-P slab, shown in Fig. 4(d).

Further effects, such as relative rotations and moiré patterns, and removing the in-plane strain we imposed to have sufficiently small supercells for computations, will compose actual experimental images. Nevertheless, the main message of our simulated STM images, presented in Figs. 4–7, is that STM appears capable of distinguishing between different phases of layered phosphorus underneath a passivating hexagonal boron nitride monolayer and it thus represents the only route known at this moment to tell these phases from one another with a local probe.

III. CONCLUSIONS

In summary, we have studied the electronic structure and simulated scanning tunnel microscopy of few-layer phosphorus allotropes capped by *h*-BN and graphene monolayers using density functional theory with vdW corrections. Our results indicate that capping by *h*-BN does permit identifying phosphorus phases underneath. Due to the vanishing band gap of graphene, the charge density of capping graphene monolayers masks the structure underneath, making this structure unsuitable to discriminate between different phosphorene allotropes. These results may assist the nascent experimental searches for different structural phases of layered phosphorus.

ACKNOWLEDGMENTS

We thank NSF-XSEDE (Grant TG-PHY090002; TACC's *Stampede*) and Arkansas (*Razor II*) for computational support. P.R. and S.B.L. acknowledge funding from the Arkansas Biosciences Institute. Z.Z., J.G., and D.T. acknowledge support by the National Science Foundation Cooperative Agreement No. EEC-0832785, titled "NSEC: Center for High-Rate Nanomanufacturing."

[1] K. S. Novoselov, D. Jiang, F. Schedin, T. J. Booth, V. V. Khotkevich, S. Morozov, and A. Geim, Proc. Natl. Acad. Sci. U.S.A. **102**, 10451 (2005).
[2] S. Z. Butler, S. M. Hollen, L. Cao, Y. Cui, J. A. Gupta, H. R. Gutiérrez, T. F. Heinz, S. S. Hong, J. Huang, A. F. Ismach *et al.*, ACS Nano **7**, 2898 (2013).
[3] P. W. Bridgman, J. Am. Chem. Soc. **36**, 1344 (1914),
[4] R. W. Keyes, Phys. Rev. **92**, 580 (1953).
[5] D. Warschauer, J. Appl. Phys. **34**, 1853 (1963).
[6] J. C. Jamieson, Science **139**, 1291 (1963).
[7] D. Schiferl, Phys. Rev. B **19**, 806 (1979).
[8] H. Asahina, K. Shindo, and A. Morita, J. Phys. Soc. Jap. **51**, 1193 (1982).
[9] H. Kawamura, I. Shirotani, and K. Tachikawa, Solid State Comm. **49**, 879 (1984).
[10] Y. Akahama, H. Kawamura, S. Carlson, T. Le Bihan, and D. Häusermann, Phys. Rev. B **61**, 3139 (2000).
[11] G. Monaco, S. Falconi, W. A. Crichton, and M. Mezouar, Phys. Rev. Lett. **90**, 255701 (2003).
[12] H. Liu, A. T. Neal, Z. Zhu, Z. Luo, X. Xu, D. Tománek, and P. D. Ye, ACS Nano **8**, 4033 (2014).
[13] L. Li, Y. Yu, G. J. Ye, Q. Ge, X. Ou, H. Wu, D. Feng, X. H. Chen, and Y. Zhang, Nat. Nanotechnol. **9**, 372 (2014).
[14] S. P. Koenig, R. A. Doganov, H. Schmidt, A. H. Castro Neto, and B. Özyilmaz, Appl. Phys. Lett. **104**, 103106 (2014).
[15] M. Buscema, D. J. Groenendijk, S. I. Blanter, G. A. Steele, H. S. J. van der Zant, and A. Castellanos-Gomez, Nano Lett. **14**, 3347 (2014).
[16] V. Tran, R. Soklaski, Y. Liang, and L. Yang, Phys. Rev. B **89**, 235319 (2014).
[17] H. O. H. Churchill and P. Jarillo-Herrero, Nat. Nanotechnol. **9**, 330 (2014).
[18] R. Fei and L. Yang, Nano Lett. **14**, 2884 (2014).
[19] A. S. Rodin, A. Carvalho, and A. H. Castro Neto, Phys. Rev. Lett. **112**, 176801 (2014).
[20] A. N. Rudenko and M. I. Katsnelson, Phys. Rev. B **89**, 201408 (2014).
[21] Q. Wei and X. Peng, Appl. Phys. Lett. **104**, 251915 (2014).
[22] J.-W. Jiang and H. S. Park, Nat. Commun. **5**, 4727 (2014).
[23] X. Peng, Q. Wei, and A. Copple, Phys. Rev. B **90**, 085402 (2014).
[24] Z. Zhu and D. Tománek, Phys. Rev. Lett. **112**, 176802 (2014).
[25] J. Guan, Z. Zhu, and D. Tománek, Phys. Rev. Lett. **113**, 046804 (2014).
[26] J. Guan, Z. Zhu, and D. Tománek, ACS Nano **8**, 12763 (2014).
[27] J. Guan, Z. Zhu, and D. Tománek, Phys. Rev. Lett. **113**, 226801 (2014).
[28] S. Bocker and M. Haser, Z. Anorg. Allg. Chem. **621**, 258 (1995).
[29] G. Seifert and E. Hernandez, Chem. Phys. Lett. **318**, 355 (2000).
[30] A. J. Karttunen, M. Linnolahti, and T. A. Pakkanen, Chem. Phys. Phys. Chem. **9**, 2550 (2008).
[31] S. E. Boulfelfel, G. Seifert, Y. Grin, and S. Leoni, Phys. Rev. B **85**, 014110 (2012).
[32] X. Han, H. M. Stewart, S. A. Shevlin, C. R. A. Catlow, and Z. X. Guo, Nano Lett. **14**, 4607 (2014).
[33] A. Castellanos-Gomez, L. Vicarelli, E. Prada, J. O. Island, K. L. Narasimha-Acharya, S. I. Blanter, D. J. Groenendijk, M. Buscema, G. A. Steele, J. V. Alvarez *et al.*, 2D Mater. **1**, 025001 (2014).
[34] J. D. Wood, S. A. Wells, D. Jariwala, K.-S. Chen, E. Cho, V. K. Sangwan, X. Liu, L. J. Lauhon, T. J. Marks, and M. C. Hersam, Nano Lett. **14**, 6964 (2014).
[35] D. Tománek, Mater. Express **4**, 545 (2014).
[36] J. Shin, K. Park, W.-H. Ryu, J.-W. Jung, and I.-D. Kim, Nanoscale **6**, 12718 (2014).
[37] S. Chen, L. Brown, M. Levendorf, W. Cai, S.-Y. Ju, J. Edgeworth, X. Li, C. W. Magnuson, A. Velamakanni, R. D. Piner *et al.*, ACS Nano **5**, 1321 (2011).
[38] T. Coan, G. S. Barroso, G. Motz, A. Bolzán, and R. A. F. Machado, Mater. Res. **16**, 1366 (2013).
[39] N. Gillgren, D. Wickramaratne, Y. Shi, T. Espiritu, J. Yang, J. Hu, J. Wei, X. Liu, Z. Mao, K. Watanabe *et al.*, 2D Mater. **2**, 011001 (2015).
[40] C. R. Dean, A. F. Young, I. Meric, C. Lee, L. Wang, S. Sorgenfrei, K. Watanabe, T. Taniguchi, P. Kim, K. L. Shepard *et al.*, Nat. Nanotechnol. **5**, 722 (2010).
[41] D. Pacilé, J. C. Meyer, C. O. Girit, and A. Zettl, Appl. Phys. Lett. **92**, 133107 (2008).
[42] C. G. Lee, Q. Li, W. Kalb, X. Liu, H. Berger, R. W. Carpick, and J. Hone, Science **328**, 76 (2010).
[43] C. R. Dean, A. F. Young, I. Meric, C. Lee, L. Wang, S. Sorgenfrei, K. Watanabe, T. Taniguchi, P. Kim, K. L. Shepard *et al.*, Nat. Mater. **5**, 722 (2010).
[44] K. K. Kim, A. Hsu, X. Jia, S. M. Kim, Y. Shi, M. Hofmann, D. Nezich, J. F. Rodriguez-Nieva, M. Dresselhaus, T. Palacios *et al.*, Nano Lett. **12**, 161 (2012).
[45] K. Watanabe, T. Taniguchi, and H. Kanda, Nat. Mater. **3**, 404 (2004).
[46] K. T. He, J. C. Koepke, S. Barraza-Lopez, and J. W. Lyding, Nano Lett. **10**, 3446 (2010).
[47] Y. Liu, F. Xu, Z. Zhang, E. S. Penev, and B. I. Yakobson, Nano Lett. **14**, 6782 (2014).
[48] T. Höltzl, T. Veszprémi, and M. T. Nguyen, C. R. Chemie **13**, 1173 (2010).
[49] E. Artacho, E. Anglada, O. Dieguez, J. D. Gale, A. García, J. Junquera, R. M. Martin, P. Ordejón, J. M. Pruneda, D. Sánchez-Portal *et al.*, J. Phys. Cond. Mat. **20**, 064208 (2008).
[50] J. Klimes, D. R. Bowler, and A. Michaelides, J. Phys. Condens. Matter **22**, 022201 (2010).
[51] N. Troullier and J. L. Martins, Phys. Rev. B **43**, 1993 (1991).
[52] Y. Du, C. Ouyang, S. Shi, and M. Lei, J. Appl. Phys. **107**, 093718 (2010).
[53] Ø. Prytz and E. Flage-Larsen, J. Phys.: Condens. Matter **22**, 015502 (2010).
[54] S. Appalakondaiah, G. Vaitheeswaran, S. Lebégue, N. E. Christensen, and A. Svane, Phys. Rev. B **86**, 035105 (2012).
[55] C. Tayran, Z. Zhu, M. Baldoni, D. Selli, G. Seifert, and D. Tománek, Phys. Rev. Lett. **110**, 176805 (2013).
[56] H. Fujihisa, Y. Akahama, H. Kawamura, Y. Ohishi, Y. Gotoh, H. Yamawaki, M. Sakashita, S. Takeya, and K. Honda, Phys. Rev. Lett. **98**, 175501 (2007).
[57] N. Ooi, A. Rairkar, L. Lindsley, and J. B. Adams, J. Phys.: Condens. Matter **18**, 97 (2006).
[58] S. Barraza-Lopez, P. M. Albrecht, N. A. Romero, and K. Hess, J. Appl. Phys. **100**, 124304 (2006).
[59] D. Tomanek and S. G. Louie, Phys. Rev. B **37**, 8327 (1988).
[60] A. Selloni, P. Carnevali, E. Tosatti, and C. D. Chen, Phys. Rev. B **31**, 2602 (1985).
[61] J. Tersoff and D. R. Hamann, Phys. Rev. Lett. **50**, 1998 (1983).
[62] J. Tersoff and D. R. Hamann, Phys. Rev. B **31**, 805 (1985).